Form Factor Comparison for Neutrino-Induced Coherent Pion Production to Constrain Neutrino Flux at DUNE

Jonathan T. Rositas*
Fermi National Accelerator Laboratory, Batavia, Illinois 60510, USA and
The University of Chicago, Chicago, Illinois, 60637, USA
(Dated: August 11, 2023)

Neutrino-induced coherent pion production is an interaction between a neutrino and a target nucleus under conditions of low momentum transfer that leaves the nucleus in the ground state. This interaction is easily reconstructed, so it is a promising candidate to constrain neutrino flux in the Deep Underground Neutrino Experiment (DUNE). However, its cross section is poorly defined due to uncertainties on the nucleon axial form factor. In this work, we have compared three form factor descriptions: a dipole approximation based on axial mass, M_A, a z power series expansion based on deuterium bubble chamber data, and z expansions for two Lattice QCD calculations. Over relevant variable ranges, the curves for the form factors as a function of momentum transfer were compared along with reweighted event data for kinematic variables in events simulated using GENIE. The relative differences between various form factors and the dipole approximation with $M_A = 1.00$ GeV were under 11%. The relative differences for the momentum transferred from the neutrino, momentum transferred to the nucleus only, and energy of the neutrino were under 13%. With this in mind, neutrino-induced coherent pion production can be used to constrain neutrino flux in DUNE within these uncertainties.

I. INTRODUCTION

There are yet a great many questions about the fundamental properties of neutrinos. Questions regarding the ordering of the mass states of the various flavors, mixing angles between the mass and flavor eigenstates, and the charge-parity violating phase abound and motivate modern neutrino experiments to search for methods by which to constrain these values. Since the number of interactions at various energies is the method by which these values intrinsic to neutrinos can be determined, it is imperative that oscillation experiments such as the Deep Underground Neutrino Experiment (DUNE) have knowledge of the energy and number distribution of neutrinos that pass through their detectors.

This energy-number distribution is known as the neutrino flux, and it is predictably difficult to get an accurate count of how many neutrinos are passing through a detector. Even if one had an estimate of how many neutrinos would be produced at the proton target upstream of the detector, due to neutrino oscillations and the wide angle of the beam, it is often difficult to determine the energy or number of neutrinos at the detector to precision levels necessary for experiments solely using beam data. Instead, neutrino flux is more effectively determined at the detector. This is done by starting with an interaction that has a well defined cross section and is "clean" enough for the detector to easily reconstruct the incident neutrino energy. If one knows the chance of an interaction occurring, the number of those interactions that occur within the detector, and the reconstructed energies of the incident neutrinos that caused these interactions, then one is able to deduce the flux at the detector.

Neutrino-electron scattering has been proposed as one of these such interactions for DUNE [1], and, while being being very well understood, this interaction suffers from a low cross section. Since high statistics are vital to neutrino experiments, it is therefore logical to consider an interaction with a greater cross section.

Neutrino-induced coherent pion production is presented as a strong candidate for this greater-cross section interaction. Although more theoretically complex than neutrino-electron scattering, it is believed that the recent advancements in theory surrounding the interaction [2–10] will allow for a neutrino flux constraint to be extracted using this process. This interaction has great potential to be used as a flux constraint since it quantifies what few approximations it utilizes, it is applicable at both low and high energies with the correct kinematic cuts employed, the effects of final state interactions are negligible [9], and the incident neutrino energy can be reconstructed to high confidence. At the same time, understanding this interaction is crucial as it is a potentially problematic background in ν_e oscillation experiments [9, 11].

The main setback with neutrino-induced coherent pion production is the uncertainty in cross section due to lack of precise knowledge of the axial form factor [2, 4, 7, 10, 12–18]. This problem has been taken on by many groups [14–17, 19–23] seeking to constrain this form factor through various methods. Since few of the results of these experiments are in total agreement with one another, it is useful to compare their respective form factors and quantify the effects of their differences on measured quantities of neutrino interactions.

In this paper, these various form factor descriptions will be laid out and explained before being directly compared with one another over the relevant momentum transfer ranges. Next, these form factors will be used

* jrositas@uchicago.edu

to reweight events simulated using the GENIE neutrino event generator to ascertain the physical manifestations predicted by the descriptions, finally an analysis and conclusion will be given on the results of the comparison.

The paper is structured in the following manner. Sec. II begins by providing background information foundational to the process of neutrino-induced coherent pion production. Next, Sec. III provides a light summary of each of the descriptions presented to determine the nucleon axial form factor. This is followed by Sec. IV where the shape of the form factor curve for each of the descriptions is explicitly laid out and directly compared to the others. Continuing to the events themselves, Sec. V uses these form factor curves to reweight GENIE data for neutrino events to determine the shape of predictions for kinematic variables under each theory. Sec. VI then points out notable trends and results from these comparisons. Finally, Sec. VII gives a summary of the work.

II. NEUTRINO-INDUCED COHERENT PION PRODUCTION

Neutrino-induced coherent pion production is an interaction between a neutrino of arbitrary flavor, ν_l, and a nucleus, N, where the products are the same nucleus, an appropriate lepton, l, and an appropriate pion, π. This interaction has both a charged-current (CC) channel,

$$\nu_l + N \to l + \pi^{\pm} + N,$$

and a neutral-current (NC) channel,

$$\nu_l + N \to \nu_l + \pi^0 + N.$$

A Feynman diagram for the CC interaction is shown in Fig. 1, and a Feynman diagram for the NC channel is shown in Fig. 2. In the NC case, the π^0 further decays into two photons that are potentially mistaken for an e^-, which is particularly relevant to ν_e oscillation experiments as a background.

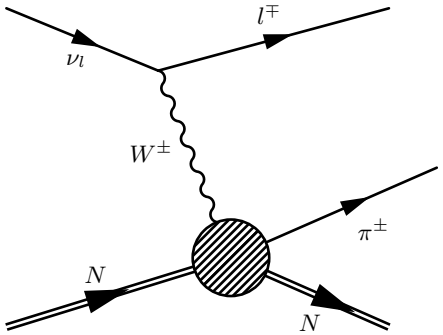

FIG. 1: Charged-Current Coherent Pion Production.

The core tenet of this interaction is the demand that the nucleus must maintain the same state before and after the interaction takes place; i.e., the quantum numbers describing the nucleus must remain unvaried throughout the interaction with the neutrino. This is what terms the interaction "coherent." Due to this constraint, coherent pion production only occurs at low four-momentum transfers between the neutrino-lepton system and the nucleus system, denoted as q. In order to analyze this variable as an invariant, q^2 is considered instead, and, since q^2 is often less than zero, $Q^2 = -q^2$ is more commonly utilized in calculations and analyses. This relationship is explicitly laid out as

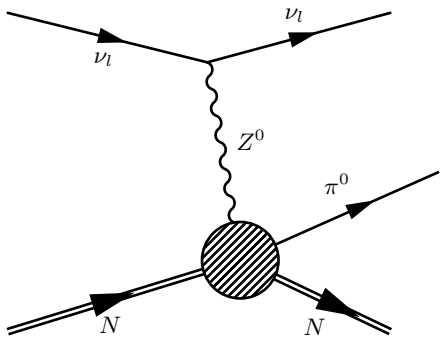

FIG. 2: Neutral-Current Coherent Pion Production.

$$Q^2 \equiv -q^2 = -(p_\nu - p_l)^2, \tag{1}$$

where p_ν is the four-momentum of the neutrino, and p_l is the four-momentum of the outgoing lepton. Only interactions under a certain Q^2 threshold are relevant for consideration for coherent pion production, which is the main kinematic cut that must be made when considering the interaction. However, while Q^2 is a useful kinematic variable for most cuts and important in determining how the neutrino will "see" the target nucleus, there is also some momentum transfer to the pion, and Q^2 fails to differentiate momentum transfer to the pion from transfer to the nucleus itself. The variable t is introduced to remedy this. It is properly the squared four-momentum transfer from the neutrino-lepton-pion system to the nucleus, which is laid out as

$$t = (p_\nu - p_l - p_\pi)^2, \tag{2}$$

where p_π is the four-momentum of the outgoing pion. This variable is the best measure of coherence, and it is useful in tandem with Q^2 for analyzing the kinematics of interactions.

The cross section for neutrino-induced coherent pion production [11, 18, 24] is given as

$$\frac{\mathrm{d}\sigma}{\mathrm{d}x\mathrm{d}y\mathrm{d}|t|} = \frac{G_F^2 m_{\mathcal{N}} f_\pi^2 E_\nu (1-y)}{2\pi^2 g_A} \times F_A(Q^2) \frac{\mathrm{d}\sigma(\pi^0 + N \to \pi^0 + N)}{\mathrm{d}|t|}, \tag{3}$$

where G_F is the Fermi coupling constant, $m_{\mathcal{N}}$ is the nucleon mass, f_π is the pion decay constant, E_ν is the energy of the incoming neutrino, $y = \frac{E_\nu - E_l}{E_\nu}$ with E_l as the energy of the outgoing lepton, g_A is the axial coupling

constant [1], $\frac{\mathrm{d}\sigma(\pi^0+N\to\pi^0+N)}{\mathrm{d}|t|}$ is the pion-nucleus cross section, and $F_A(Q^2)$ is the nucleon axial form factor, which is known to be a function of Q^2.

All variables other than the pion-nucleus cross section and $F_A(Q^2)$ are known to high confidence. Accordingly, these two variables must be constrained to calculate the coherent pion production cross section. The pion-nucleus cross section can be directly measured by DUNE, so it is expected that this value will come into focus through experiments in the coming years. Conversely, $F_A(Q^2)$ can only be directly measured through measurements on free nucleons, which cannot be done within DUNE. Due to the difficulty of conducting such an experiment, $F_A(Q^2)$ must instead be determined by using data from other experiments and through theory, and these proposed values must be rigorously cross examined to determine the most accurate description for $F_A(Q^2)$. Descriptions offering answers to the question of the shape of $F_A(Q^2)$ will now be laid out in the following section.

III. DISCUSSION OF FORM FACTOR DESCRIPTIONS

Descriptions for $F_A(Q^2)$ range from rough approximations to complex parameterizations. No matter the idea, all descriptions must, in some way, consider the data from the bubble chamber experiments from Argonne National Laboratory (ANL), [20–22], Brookhaven National Laboratory (BNL) [19], and Fermi National Accelerator Laboratory (FNAL) [23] that provide experimental data to constrain the form of $F_A(Q^2)$.

A. Axial Dipole Approximation

The simplest of the models for $F_A(Q^2)$ is the dipole approximation. This model is rigorously defined in Refs. [4–7, 15], and is treated as an assumption that, while known to be imperfect, is a reasonable fit at low Q^2 where $F_A(Q^2)$ is relevant to coherent pion production. The equation for the dipole approximation is given as

$$F_A^{\mathrm{Dip}}(Q^2) = \frac{g_A}{(1+\frac{Q^2}{M_A^2})^2} \tag{4}$$

where g_A is the axial coupling constant, and M_A is the axial mass.

While $F_A^{\mathrm{Dip}}(Q^2)$ is only dependent on a single unknown quantity, the value of M_A is poorly constrained by experiments, which raises reasonable doubts that $F_A^{\mathrm{Dip}}(Q^2)$ is an oversimplified model and should not be used as the description for $F_A(Q^2)$. M_A has been measured [19–23] for decades now, but there still exist severe tensions between various experiments, with the only strong consensus being that $1.00\ \mathrm{GeV} \leq M_A \leq 1.40\ \mathrm{GeV}$. Even over this seemingly small range, these different values for M_A generate quite different curves for $F_A^{\mathrm{Dip}}(Q^2)$ as will be shown in Sec. IV A. Nevertheless, the relatively simple expression for $F_A^{\mathrm{Dip}}(Q^2)$ combined with the research done in the past [19–23, 26] make the dipole approximation a good baseline for $F_A(Q^2)$ in flux constraint considerations.

[1] In the dipole approximation, $g_A = 1.2723$ as defined in Ref.[25]. However, the other descriptions may use slightly different values for g_A.

B. z Expansion

In response to the simple, but poorly constrained, dipole approximation model description, the z expansion presents a method of defining $F_A(Q^2)$ independently of any model. Instead of considering the physical distribution of $F_A(Q^2)$, the z expansion employs a power series expansion to fit the shape of $F_A(Q^2)$. A proper mathematical treatment of this theory is given in Refs. [2, 3, 14], but a brief description similar to that in Ref.[12] will also be given here.

In Quantum Chromodynamics (QCD), the function $F_A(Q^2)$ is analytic for $Q^2 = -t > -t_{\mathrm{cut}}$ where t_{cut} denotes the location of a t-channel cut. Therefore, a new analytic function $z(Q^2)$ can be defined:

$$z(Q^2) = \frac{\sqrt{t_{\mathrm{cut}}+Q^2} - \sqrt{t_{\mathrm{cut}}-t_0}}{\sqrt{t_{\mathrm{cut}}+Q^2} + \sqrt{t_{\mathrm{cut}}-t_0}} \tag{5}$$

with t_0 as a somewhat arbitrary parameter that collaborations utilizing descriptions based on the z expansion formalism will define differently. In all examinations, t_{cut} is chosen to be $t_{\mathrm{cut}} \equiv (3m_\pi)^2$, which is the three-pion kinematic threshold [16]. $F_A(Q^2)$ can now be expanded as a power series in $z(Q^2)$ since $|z| < 1$:

$$F_A^z(Q^2) = \sum_{k=0}^{\infty} a_k z(Q^2)^k \approx \sum_{k=0}^{k_{max}} a_k z(Q^2)^k, \tag{6}$$

which can in turn be truncated to an approximation by only running the summation over a finite number of coefficients as shown in Eq. 6.

There have been two families of endeavors to determine the values of a_k: experimentally, by using deuterium data, and theoretically, by using Lattice Quantum Chromodynamics calculations. Both of these methods will be addressed in the following two subsections.

1. Deuterium Data

Using a fit to the bubble chamber experiments' data [19–23], Ref. [14] constrains a_k as shown in Table I.

a_0	a_1	a_2	a_3	a_4
0.759	-2.30	0.6	3.8	-2.3

a_5	a_6	a_7	a_8
-2.16	0.896	1.58	-0.823

TABLE I: Coefficients for the deuterium data z expansion fit to the combined datasets from all bubble chamber experiments [19–23].

It is important to note that Ref. [14] defines all coefficients based on $F_A(q^2)$, so the coefficients given in that work have had their signs switched to be compatible with $F_A(Q^2)$.

For this implementation of the z expansion description, t_0 was chosen in order to minimize $|z|$ over the range 0.00 GeV^2 $\leq Q^2 \leq$ 1.00 GeV^2. This value was determined explicitly as

$$t_0 \equiv t_{\rm cut}(1 - \sqrt{1 + (Q^2_{\rm max}/t_{\rm cut})} \approx -0.28{\rm GeV}^2. \quad (7)$$

Fits were performed to each set of data independently, but the coefficients given in Table I are for a simultaneous fit to the combined data set from all bubble chamber experiments.

2. Lattice QCD

As Lattice QCD (LQCD) has seen improvements over the past decade, there has been intense interest in constraining $F_A(Q^2)$ through theoretical calculations employing the z expansion description. In this work, Lattice QCD calculations from two groups were analyzed, one from Bali *et al.* [15] and one from Djukanovic *et al.* [16].

For the calculations done by Bali *et al.*, the coefficients specifically for their $!z^{4+3}$ calculation were utilized as they remark that this calculation gave the best description of their data. These coefficients are given in Table II.

a_0	a_1	a_2	a_3	a_4	a_5	a_6
1.013	-1.713	-0.591	-0.771	7.790	-8.418	2.689

TABLE II: Coefficients from LQCD calculations done by Bali *et al.* [15].

For t_0, they define

$$t_0 = -t_{\rm cut} = -9m_\pi^2, \quad (8)$$

which was chosen such that the function was well-behaved at $t_{\rm cut} = t_0$.

The coefficients for Djukanovic *et al.* are given in Table III.

a_0	a_1	a_2
1.225	-1.274	-0.379

TABLE III: Coefficients from LQCD calculations done by Djukanovic *et al.* [16].

They never explicitly define t_0, instead defining z as

$$z(Q^2) = \frac{\sqrt{t_{cut} + Q^2} - \sqrt{t_{cut}}}{\sqrt{t_{cut} + Q^2} + \sqrt{t_{cut}}}. \quad (9)$$

However, it can be noted that this is the same as the z definition from the other works with $t_0 = 0$.

Now that all of the parameters regarding the various descriptions of $F_A(Q^2)$ have been defined, direct comparisons and visualizations of the behavior of $F_A(Q^2)$ for these descriptions will be presented in the following section.

IV. AXIAL FORM FACTOR COMPARISON

We made a direct comparison of the shapes of the $F_A(Q^2)$ curves for each description in order to assess the magnitude of variation between them. These descriptions were first analyzed within their own families and later compared comprehensively against all other descriptions. Two ranges of Q^2 were used for these analyses, both starting at $Q^2_{\rm min} = 0.00$ GeV^2 but with $Q^2_{\rm max} = 1.00$ GeV^2 for a greater picture of how the descriptions differ at larger values of Q^2 and $Q^2_{\rm max} = 0.20$ GeV^2 for a tighter comparison over the values of Q^2 that are more relevant to coherent pion production.

A. Dipole Approximation

To analyze the dipole approximation description, various values of M_A were used to generate the $F_A(Q^2)$ curves. These values were selected to range from 1.00 GeV^2 to 1.25 GeV^2 in increments of 0.05 GeV^2. The plots to the different maximum values of Q^2 are given in Fig. 3.

To better quantify the differences over both ranges of Q^2, a plot of the the dipole approximation with different values for M_A were compared against the dipole approximation with $M_A = 1.00$ GeV according to

$$|\Delta F_A^i(Q^2)| = \frac{|F_A^i(Q^2) - F_A^{\rm Dip.,\, M_A=1.00}(Q^2)|}{|F_A^{\rm Dip.,\, M_A=1.00}(Q^2)|}, \quad (10)$$

where $\Delta F_A^i(Q^2)$ is the relative difference for a given from factor description, $F_A^i(Q^2)$, and $F_A^{\rm Dip.,\, M_A=1.00}(Q^2)$ is the $F_A(Q^2)$ for the dipole approximation with $M_A = 1.00$ GeV, which was chosen arbitrarily. The results are shown in Fig. 4.

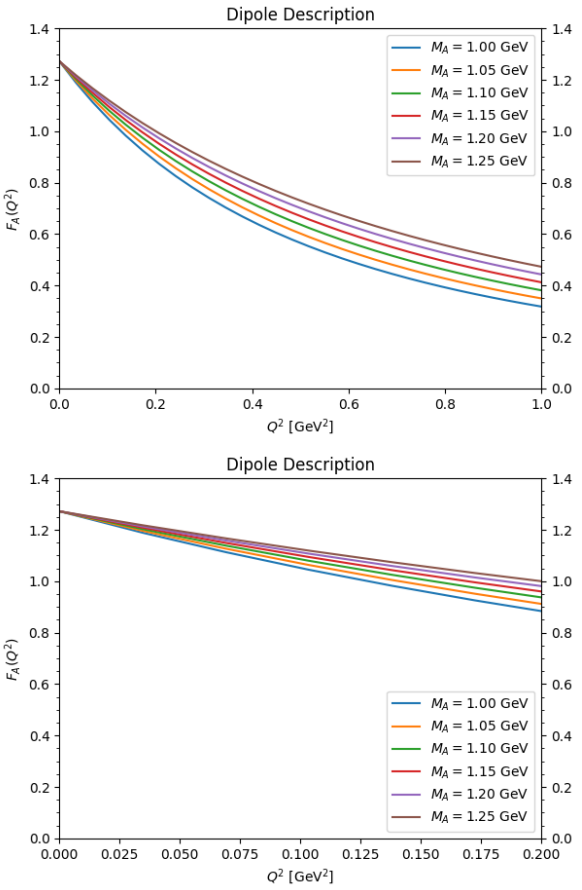

FIG. 3: Comparisons of $F_A(Q^2)$ for the dipole approximation descriptions with varying values of M_A. $Q^2_{\text{max}} = 1.00$ GeV^2 for the top figure and $Q^2_{\text{max}} = 0.20$ GeV^2 for the bottom figure.

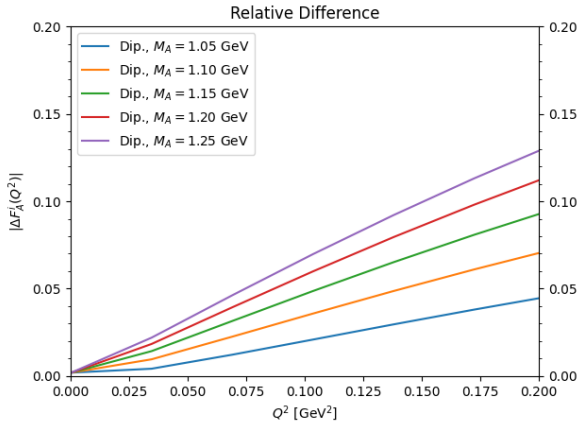

FIG. 4: Relative difference plot for varying values of M_A for the dipole approximation description. $M_A = 1.00$ GeV is the baseline. $Q^2_{\text{max}} = 0.20$ GeV^2 since the trends continue linearly past the relevant range.

B. z Expansion

Beginning the comparisons of the z expansion descriptions with the deuterium data study, the shape of the axial form factor, $F_A^{z,\text{D}}(Q^2)$, curves for varying values of k_{max} were examined. This analysis is shown in Fig. 5.

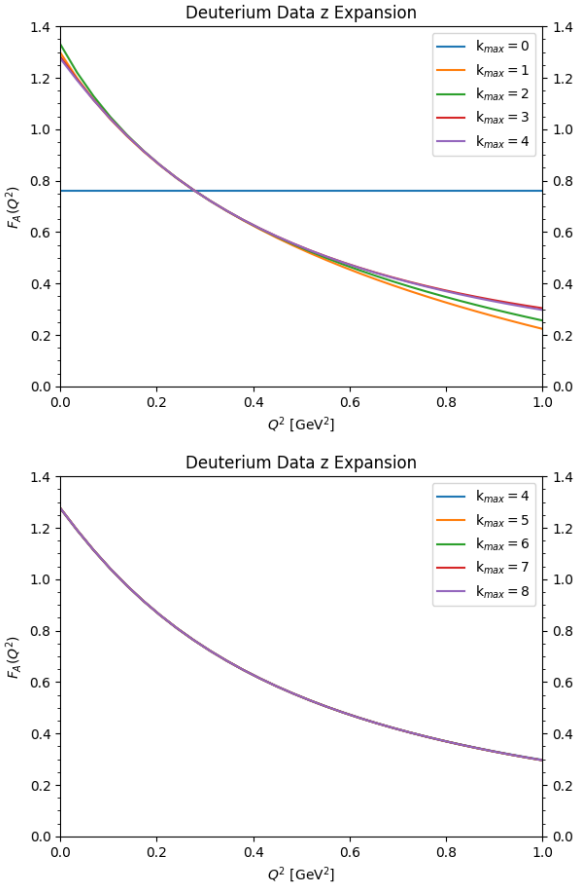

FIG. 5: Comparisons of $F_A(Q^2)$ for the deuterium data z expansion description with varying values of k_{max}. These curves are plotted to $Q^2_{\text{max}} = 1.00$ GeV^2 in order to better show the subtle differences as k_{max} increases.

Similarly to as is done in Ref. [14], it was noted that the $F_A^{z,\,\text{D}}(Q^2)$ curve for $k_{\text{max}=4}$ is essentially the same as for greater values of k_{max}. This was proven through a relative difference plot generated using an expression similar to Eq. 10:

$$|\Delta F_A^i(Q^2)| = \frac{|F_A^i(Q^2) - F_A^{z,\,\text{D},\,k_{\text{max}}=4}(Q^2)|}{|F_A^{z,\,\text{D},\,k_{\text{max}}=4}(Q^2)|}, \qquad (11)$$

where $F_A^i(Q^2)$ is now one of the $F_A^{z,\,\text{D}}(Q^2)$ curves for the deuterium data z expansion except for $k_{\text{max}} = 0$ due to it being an unhelpful description and $k_{\text{max}} = 4$ because $F_A^{z,\,\text{D},\,k_{\text{max}}=4}(Q^2)$ is the $F_A(Q^2)$ curve for the deuterium data z expansion with $k_{\text{max}=4}$, which is used as the baseline for the relative difference analysis.

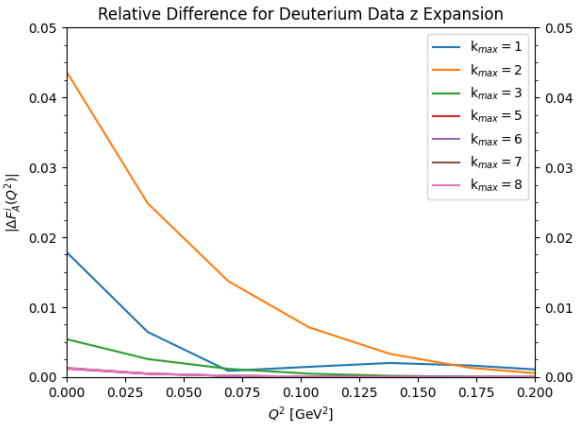

FIG. 6: Relative difference plot for varying values of $k_{\max}$ for the deuterium data z expansion. $k_{\max} = 4$ is the baseline. The curve for $k_{\max} = 0$ has been purposely omitted.

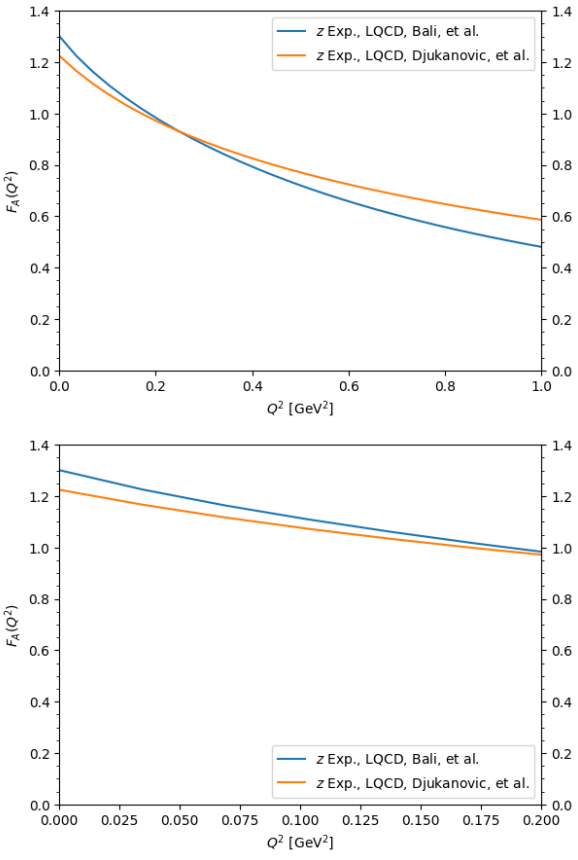

FIG. 7: Comparisons of $F_A(Q^2)$ for both LQCD z expansion descriptions. $Q^2_{\max} = 1.00$ GeV^2 for the top figure and $Q^2_{\max} = 0.20$ GeV^2 for the bottom figure.

As can be seen from Fig. 6, $F_A^{z,\,\mathrm{D}}(Q^2)$ for $k_{\max} = 4$ is an accurate description of the results of the bubble chamber study. Therefore, $F_A^{z,\,\mathrm{D}}(Q^2)$ was used exclusively with $k_{\max} = 4$ throughout the rest of this examination for the sake of simplicity.

Moving to the LQCD calculations carried out by Bali *et al.* [15] and Djukanovic *et al.* [16], the coefficients are calculated such that it would be improper not to use the entire list calculated by each collaboration, so there is no need to independently determine what $k_{\max}$ should be for these descriptions. Figure 7 shows $F_A(Q^2)$ for these two descriptions. One can see that these descriptions do not converge to g_A at $F_A(Q^2 = 0)$ as is expected and shown in the other descriptions. This is due to the uncertainties intrinsic to the calculations, and the difference in the spectra is likely not a real effect.

C. Direct Comparison

Finally for $F_A(Q^2)$, selected descriptions from all families were compared at once. In order to get a range of values for the dipole approximation without crowding the plots, only dipole descriptions with $M_A = 1.00, 1.10, 1.20$ GeV were plotted. Once again, these descriptions were all compared over both $Q^2_{\max} = 1.00$ GeV^2 and $Q^2_{\max} = 0.20$ GeV^2. Figure 8 shows both of these comparisons.

In order to more precisely analyze the differences between the $F_A(Q^2)$ descriptions, a relative difference plot was generated according to Eq. 10, where $F_A^i(Q^2)$ is any selected form factor description, not simply any dipole approximation description as in Sec. IV A. Figure 9 shows these relative differences only to $Q^2_{\max} = 0.20$ GeV^2 as it is more easily seen that the descriptions differ appreciably at greater values of Q^2.

V. EVENT REWEIGHTING

In order to get an idea of how these changes in $F_A(Q^2)$ would manifest within the detector, it was necessary to compare event variables as recorded by the detector for different descriptions. This was facilitated principally by generating 1,000,000 events using the detector geometry of the DUNE Near Detector in GENIE with $F_A(Q^2)$ given by the dipole approximation with $M_A = 1.00$ GeV. The events from this file were then reweighted according to their Q^2 value for the other $F_A(Q^2)$ descriptions to compare the shapes of event distributions. Figure 10 gives three histograms of various reweighted event distributions for event variables.

Furthermore, Fig. 11 shows the relative differences between reweighted number of events in each bin for each $F_A(Q^2)$ for each variable. The method for generating these curves is given as

$$|\Delta N_a^i(\zeta, Q^2)| = \frac{|N_a^i(\zeta, Q^2) - N_a^{\mathrm{Dip.},\,M_A=1.00}(\zeta, Q^2)|}{|N_a^{\mathrm{Dip.},\,M_A=1.00}(\zeta, Q^2)|}, \tag{12}$$

where $\Delta N_a^i(\zeta)$ is the relative difference in the reweighted number, N, of events in a bin, a, for an arbitrary variable, ζ, with an arbitrary form factor description that is

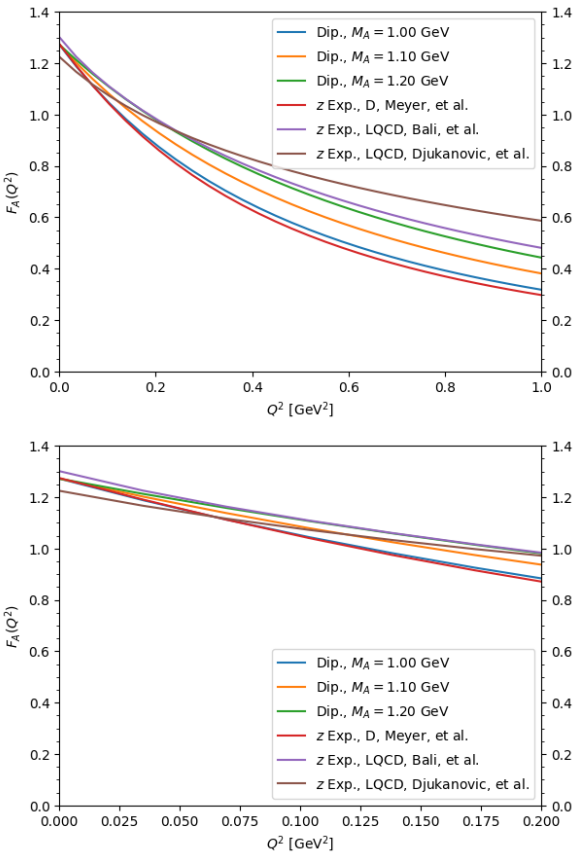

FIG. 8: Comparisons of $F_A(Q^2)$ for the dipole description with selected M_A values and the z expansion description for the deuterium data [14], LQCD calculations by Bali *et al.* [15], and LQCD calculations by Djukanovic *et al.* [16]. $Q^2_{\rm max} = 1.00$ GeV^2 for the top figure and $Q^2_{\rm max} = 0.20$ GeV^2 for the bottom figure.

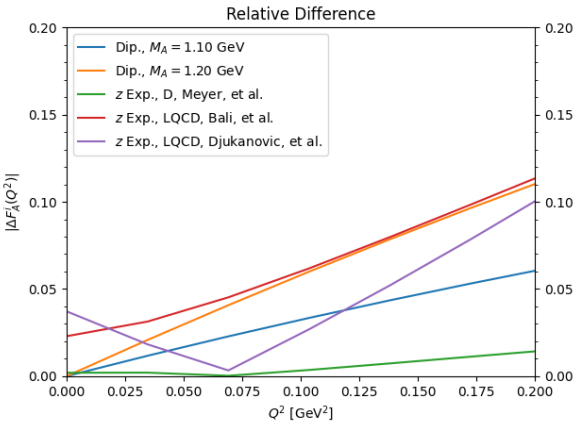

FIG. 9: Relative difference as given in Eq. 10 between selected $F_A(Q^2)$ descriptions and the $F_A(Q^2)$ curve for the arbitrarily chosen dipole approximation with $M_A = 1.00$ GeV.

still dependent on Q^2, and $N_a^{\rm Dip.,\, M_A=1.00}(\zeta, Q^2)$ repre-

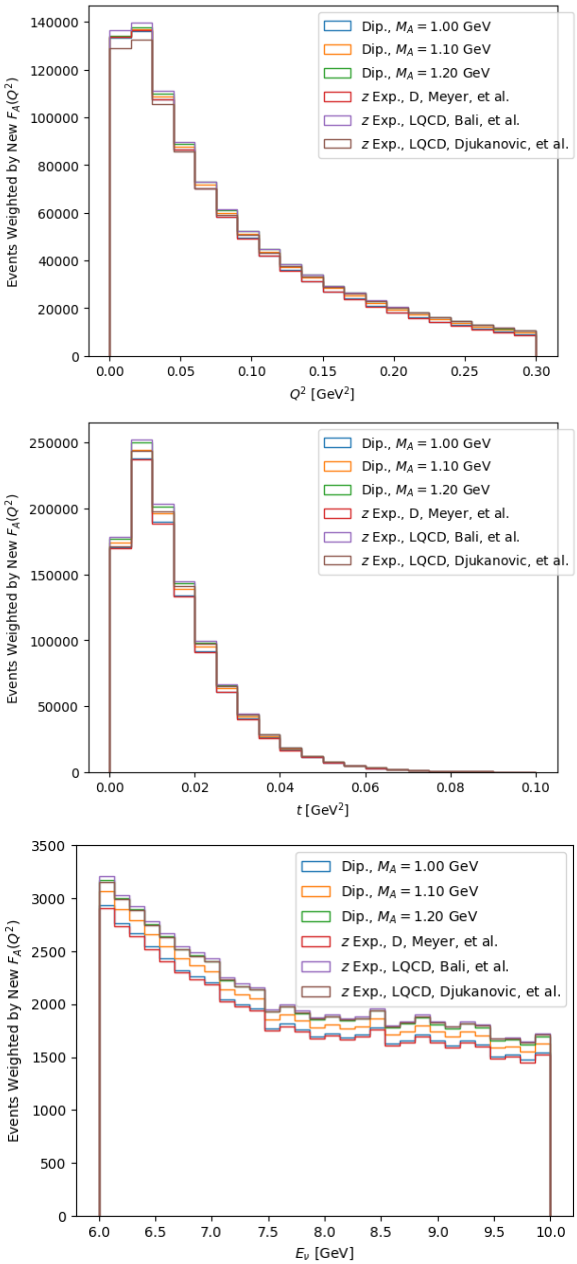

FIG. 10: Reweighted histograms for various event variables.

sents the same information but specifically for the dipole approximation description with $M_A = 1.00$ GeV^2.

VI. ANALYSIS

As seen from Fig. 9, the curves of $F_A(Q^2)$ vary only up to about 11% from the dipole approximation with $M_A = 1.00$ GeV. These uncertainties are relatively small, but the more telling indication of the sensitivity of the coherent pion production cross section is the examination of the relative difference curves for the kinematic

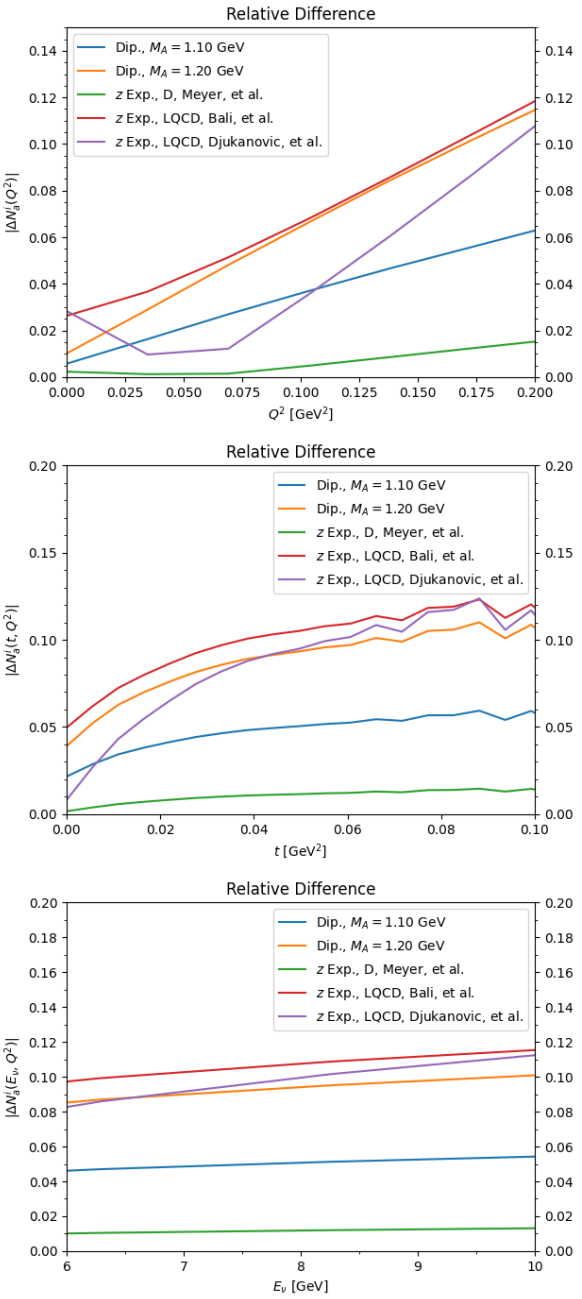

FIG. 11: Relative differences between the number of reweighted events for various event variables.

variables as presented in Fig. 11. For all three of these variables within their relevant ranges, the relative differences stay under 13%. While the curves for t grow and plateau around 0.02 GeV^2 and the curves for E_ν remain essentially flat, the Q^2 relative difference curves show rapid growth at approximately 0.100 GeV^2. Beneath that threshold for Q^2, the relative differences are even smaller, remaining under 8%. This provides evidence that, at very low values of Q^2, events exhibit only minimal kinematic differences.

VII. SUMMARY

Neutrino-induced coherent pion production is a low-momentum transfer candidate interaction to constrain neutrino flux in the DUNE Near Detector. In order for this interaction to be considered a viable candidate for flux constraint, its uncertainties regarding its cross section must be analyzed. The principle uncertainty to be addressed prior to the start of data collection at DUNE is that of the correct description of the nucleon axial form factor as a function of momentum transfer from the neutrino, $F_A(Q^2)$, over the low range of momentum transfer from the neutrino, Q^2, relevant to coherent pion production.

In this Paper, we have addressed and compared two general types of $F_A(Q^2)$ descriptions. Firstly, there is the dipole approximation. Dependent only on the value of the axial mass, M_A, this approximation is the simplest description of all that were analyzed, but it involves a great deal of uncertainty due to this axial mass parameter that experiments [19–23] offer differing values for. Secondly, there is the z expansion parameterization. This is a model-independent description that uses coefficients in a power series expansion to give the shape of the $F_A(Q^2)$ curve. Two methods of determining these coefficients in the z expansion have been analyzed here: experimentally from bubble chamber data [14] and theoretically from Lattice QCD calculations [15, 16].

All types of descriptions had their $F_A(Q^2)$ curves compared within their families (Figs. 3, 4, 5, 6, and 7) before being directly compared to one another (Figs. 8 and 9) through plotting the relative difference between various descriptions. Following this direct comparison, histograms for events generated using GENIE with the DUNE Near Detector geometry for Q^2, momentum transfer to the nucleus, and neutrino energy were reweighted according to the various form factors (Fig. 10) before the number of events in each bin also had their relative differences compared (Fig. 11).

Within the relevant range of 0.00 GeV $\leq Q^2 \leq$ 0.20 GeV^2, the relative difference between all other form factors and the dipole approximation with $M_A = 1.00$ GeV was less than 11%. Within their respective relevant ranges, the relative differences between the event variables was under 13%. Imposing a more restrictive cut, the relative difference in events for Q^2 can be reduced to less than 8% for 0.00 GeV$^2 \leq Q^2 \leq$ 0.10 GeV^2. Using this analysis, neutrino-induced coherent pion production can be used to constrain neutrino flux in the DUNE Near Detector within the uncertainties shown here. This work would benefit from a further study quantifying these differences through performing Monte Carlo template fits for these $F_A(Q^2)$ descriptions.

ACKNOWLEDGEMENTS

I would like to thank Moon Jung for providing foundational code for this project, Gray Putnam for guidance and explanation, and, with utmost gratitude, Vishvas Pandey for advising, revision, and invaluable pedagogy. This manuscript has been authored by Fermi Research Alliance, LLC under Contract No. DE-AC02-07CH11359 with the U.S. Department of Energy, Office of Science, Office of High Energy Physics. This work was supported in part by the U.S. Department of Energy, Office of Science, Office of Workforce Development for Teachers and Scientists (WDTS) under the Science Undergraduate Laboratory Internships Program (SULI).

[1] C. M. Marshall, K. S. McFarland, and C. Wilkinson, Phys. Rev. D **101**, 032002 (2020), arXiv:1910.10996 [hep-ex].

[2] B. Bhattacharya, R. J. Hill, and G. Paz, Phys. Rev. D **84**, 073006 (2011), arXiv:1108.0423 [hep-ph].

[3] R. J. Hill and G. Paz, Model independent extraction of the proton charge radius from electron scattering, Phys. Rev. D **82**, 113005 (2010), arXiv:1008.4619 [hep-ph].

[4] I. D. Kakorin, K. S. Kuzmin, and V. A. Naumov, Eur. Phys. J. C **81**, 1142 (2021), arXiv:2112.13745 [hep-ph].

[5] H. S. Budd, A. Bodek, and J. Arrington, in *2nd International Workshop on Neutrino-Nucleus Interactions in the Few GeV Region* (2003) arXiv:hep-ex/0308005.

[6] A. Bodek, H. S. Budd, and J. Arrington, AIP Conf. Proc. **698**, 148 (2004), arXiv:hep-ex/0309024.

[7] V. Bernard, L. Elouadrhiri, and U.-G. Meissner, J. Phys. G **28**, R1 (2002), arXiv:hep-ph/0107088.

[8] E. A. Paschos, A. Kartavtsev, and G. J. Gounaris, Phys. Rev. D **74**, 054007 (2006), arXiv:hep-ph/0512139.

[9] E. A. Paschos and D. Schalla, Phys. Rev. D **80**, 033005 (2009), arXiv:0903.0451 [hep-ph].

[10] A. S. Meyer, A. Walker-Loud, and C. Wilkinson 10.1146/annurev-nucl-010622-120608 (2022), arXiv:2201.01839 [hep-lat].

[11] D. I. Scully, *Neutrino induced coherent pion production.*, Ph.D. thesis, Warwick U. (2013).

[12] D. Simons, N. Steinberg, A. Lovato, Y. Meurice, N. Rocco, and M. Wagman, (2022), arXiv:2210.02455 [hep-ph].

[13] J. Nieves, I. Ruiz Simo, and M. J. Vicente Vacas, Phys. Lett. B **707**, 72 (2012), arXiv:1106.5374 [hep-ph].

[14] A. S. Meyer, M. Betancourt, R. Gran, and R. J. Hill, Phys. Rev. D **93**, 113015 (2016), arXiv:1603.03048 [hep-ph].

[15] G. S. Bali, L. Barca, S. Collins, M. Gruber, M. Löffler, A. Schäfer, W. Söldner, P. Wein, S. Weishäupl, and T. Wurm (RQCD), JHEP **05**, 126, arXiv:1911.13150 [hep-lat].

[16] D. Djukanovic, G. von Hippel, J. Koponen, H. B. Meyer, K. Ottnad, T. Schulz, and H. Wittig, Phys. Rev. D **106**, 074503 (2022), arXiv:2207.03440 [hep-lat].

[17] S. Park, R. Gupta, B. Yoon, S. Mondal, T. Bhattacharya, Y.-C. Jang, B. Joó, and F. Winter (Nucleon Matrix Elements (NME)), Phys. Rev. D **105**, 054505 (2022), arXiv:2103.05599 [hep-lat].

[18] D. Rein and L. M. Sehgal, Nucl. Phys. B **223**, 29 (1983).

[19] N. J. Baker, A. M. Cnops, P. L. Connolly, S. A. Kahn, H. G. Kirk, M. J. Murtagh, R. B. Palmer, N. P. Samios, and M. Tanaka, Phys. Rev. D **23**, 2499 (1981).

[20] W. A. Mann, U. Mehtani, B. Musgrave, Y. Oren, P. A. Schreiner, R. Singer, H. Yuta, R. Ammar, S. Barish, Y. Cho, M. Derrick, R. Engelmann, and L. G. Hyman, Phys. Rev. Lett. **31**, 844 (1973).

[21] S. J. Barish, J. Campbell, G. Charlton, Y. Cho, M. Derrick, R. Engelmann, L. G. Hyman, D. Jankowski, A. Mann, B. Musgrave, P. Schreiner, P. F. Schultz, R. Singer, M. Szczekowski, T. Wangler, H. Yuta, V. E. Barnes, D. D. Carmony, A. F. Garfinkel, and G. M. Radecky, Phys. Rev. D **16**, 3103 (1977).

[22] K. L. Miller, S. J. Barish, A. Engler, R. W. Kraemer, B. J. Stacey, M. Derrick, E. Fernandez, L. Hyman, G. Levman, D. Koetke, B. Musgrave, P. Schreiner, R. Singer, A. Snyder, S. Toaff, D. D. Carmony, G. M. Radecky, V. E. Barnes, A. F. Garfinkel, R. Ammar, D. Coppage, D. Day, R. Davis, N. Kwak, and R. Stump, Phys. Rev. D **26**, 537 (1982).

[23] T. Kitagaki *et al.*, Phys. Rev. D **28**, 436 (1983).

[24] H. Sogarwal and P. Shukla, Nucl. Phys. A **1027**, 122494 (2022), arXiv:2205.06642 [hep-ph].

[25] C. Patrignani *et al.* (Particle Data Group), Review of Particle Physics, Chin. Phys. C **40**, 100001 (2016).

[26] M. A. Ramírez *et al.* (MINERvA), (2022), arXiv:2210.01285 [hep-ex].